The International Journal of Advanced Manufacturing Technology (2023) 124:1017–1039
https://doi.org/10.1007/s00170-022-10436-4

ORIGINAL ARTICLE

Warpage and residual stress analyses of post-mold cure process of IC packages

Ming-Yu Lin[1] · Yong-Jie Zeng[1] · Sheng-Jye Hwang[1] · Ming-Han Wang[2] · Hui-Ping Liu[2] · Chin-Lung Fang[2]

Received: 6 April 2022 / Accepted: 3 November 2022 / Published online: 28 November 2022
© The Author(s) 2022

Abstract
To improve the production yield rate, reliability is one of the important indicators of electronic packaging products. In past research, however, the influence of the fabrication process was rarely taken into consideration. In this thesis, mold flow analysis software Moldex3D is used to develop a series analysis procedure for IC package products. The effects of many factors, including process, structure, and materials were being taken into account. Especially for epoxy molding compound, namely EMC, is studied on its properties during the molding and post-mold cure (PMC) processes. This paper adopted *P–V-T-C* equations, which consider both volume shrinkage due to thermal mismatch and chemical shrinkage to predict the amount of warpage and residual stresses after the mold filling process. Next, dual shift factor model for viscoelastic analysis was used to model the PMC process and predict the amount of warpage and residual stresses after PMC. And the influence of different PMC process conditions and loading conditions on the warpage results is discussed. The residual stresses after PMC simulation are set as the initial conditions for reliability analysis and then the stress distribution after two thermal cycles is analyzed. It is observed that the deformed shape of the simulation and experiment results after PMC were consistent. Both are concave downwards. In comparison with experiment results, the error of warpage simulation results was between 10% and 50%. The biggest error was found in the short direction. During two thermal cycles, it is can be found that the maximum stress of the lead frame is 505.7 MPa and the location of the possible failure is at the top left of the die. In addition, when considering or not considering the process-induced residual stress in the thermal cycle analysis, the stress states are very different.

Keywords IC package · Residual stress · *P–V-T-C* · Viscoelasticity

1 Introduction

IC encapsulation can be divided into die saw, die bonding, wire bonding, molding, molding, post-mold cure, trim, marking, plating, and inspection. For the molding and post-mold cure (PMC) of IC encapsulation process, warpage and residual stress are critical issues, especially when the package has higher density and its thinness is thin. Then solder failure, crack, and delamination are the major reliability concerns for electronic products. During the transfer molding process, epoxy molding compound (EMC) is heated and filled into the mold cavity, and then cross-linking reaction in high temperature occurs and makes the thermosetting material cured and solidified. If EMC is not fully cured after the molding process, IC packages will be put into the oven and pressed for long-term high-temperature baking to make EMC fully cured. This step is called PMC process and makes the mechanical behavior and reliability of IC packages more stable.

As shown in Fig. 1, the main reason for warpage is uneven volume shrinkage or residual stress during manufacturing. There are two main reasons for the shrinkage phenomenon, one is curing volume shrinkage of material in the mold cavity due to chemical reaction of EMC, and another one is thermal volume shrinkage of coefficient of thermal expansion (CTE) mismatch of the components' material during the cooling process.

In the previous studies, thermal shrinkage induced by different CTE values between materials was considered as the main reason for the warpage problem. However, in recent years, there are more evidence showing that the

✉ Sheng-Jye Hwang
jimppl@mail.ncku.edu.tw

[1] Department of Mechanical Engineering, National Cheng Kung University, Tainan, Taiwan

[2] ChipMOS Technologies Inc, Tainan, Taiwan

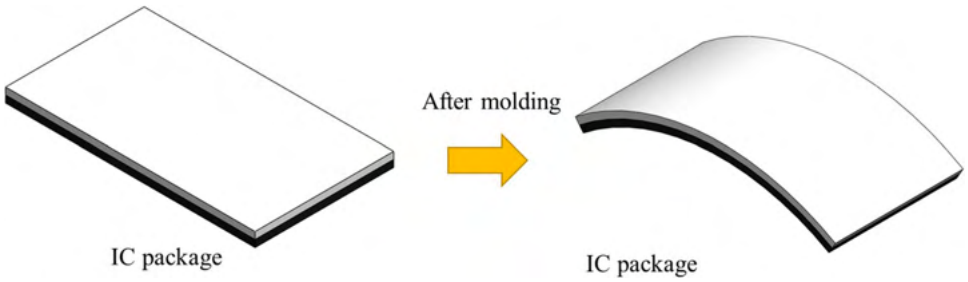

Fig. 1 Warpage problem

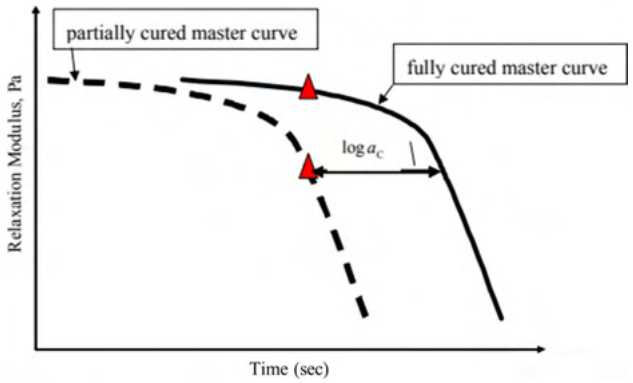

Fig. 2 Cure curve schematic [8]

cure-induced shrinkage effect cannot be ignored. Kelly et al. [1, 2] predicted warpage by considering thermal-induced and cure-induced shrinkage of EMC. Chang and Hwang [3, 4] established a relationship between pressure, volume, temperature, and conversion of thermoset material, namely, *P–V-T-C* equation. Hong and Hwang [5] used the *P–V-T-C* relation to predict the warpage of bi-material after the molding process by mold flow analysis and finite element method (FEM). Teng [6] and Deng [7] considered both thermal and cure shrinkage to predict the warpage of IC package products (TSOP, LQFP, and FOWLP) by FEM, and verified the *P–V-T-C* relation by experiments. The results show that considering both temperature effect and chemical effect can more accurately predict package warpage.

Because of the high-temperature process, EMC would behave as a viscoelastic material during the PMC process. For this reason, it is necessary to take the viscoelastic properties of the material into consideration in the PMC analysis. As shown in Fig. 2, Wang [8] and Lin [9] used dynamic mechanical analysis (DMA) and time–temperature superposition (TTS) to verify WLF equation and generalized Maxwell viscoelastic model of EMC are available. Viscoelastic properties of EMC would be determined under different temperatures by using temperature shift factor. Similarly, the cure shift factor is determined by the same approach. Combined with the shift factors, the dual shift factors are defined to obtain the relaxation modulus at any temperature and degree of cure. Therefore, the viscoelastic model with time, temperature, and conversion as its parameters were established. In order to describe the warpage and residual stress caused by the effects of EMC during molding and PMC, Wang et al. [10] analyzed the warpage of the bi-material strip. Considering the *P–V-T-C* and viscoelastic properties, the influence of curing and PMC processes are discussed. Guo [11] considered *P–V-T-C* effect of the molding process, the viscoelastic effect of PMC process, and residual stress when performing the simulation analysis. Compared with the experiment results of the actual IC package products, the experiment results were close to the simulation results.

Fatigue is defined as the process of progressive or permanent structural change occurring when materials subjected to some conditions such as thermal cycle which may lead to cracks or fracture finally. The life of IC packages can be predicted by reliability analysis. The data required for reliability analysis including plastic strain, creep, strain energy, etc. Then, select a suitable fatigue model to analyze reliability of IC packages.

Coffin proposed the Coffin-Manson model in 1954, which uses plastic strain as damage information to predict fatigue life [12]. Shi found that the fatigue ductility coefficient and fatigue ductility exponent in the model are not constants, but were affected by temperature and frequency [13]. Englemaier combined the cycle frequency, solder ball, and substrate temperature parameters to modified Coffin-Manson model. The modified model is also called the Modified Coffin-Manson model [14]. Lin used FEM and temperature cycling test (TCT) to perform two-dimensional (2D) and three-dimensional (3D) nonlinear analysis on the fatigue behavior of BGA solder balls [15]. Darveaux [16] developed a method to predict the fatigue life during the thermal cycle with crack growth experiment data. With the accumulated damage, the properties of materials do not remain the same but change all the time. Consequently, it is important to study the mechanism of damage accumulation in the material. In 1956, Miner proposed the approach of using stress amplitude to superposition the damage of materials under fatigue cycles [17]. Hamasha et al. [18] proved that Miner's rule is not available for predicting fatigue life because of two

main reasons: one is solder material is stress-dependent, and another one is that damage accumulated could be changed by previously applied stress. Su et al. [19] reviewed and categorized the fatigue models into four groups based on the critical factor which lead to fatigue damage: plastic strain-based fatigue model, damage accumulation-based fatigue model, creep damage-based fatigue model, and energy-based fatigue model.

Although there are many life prediction methods have been proposed and tried to predict fatigue life from various aspects, the fatigue mechanism of materials is too complex and difficult to predict, which limits these fatigue models. Therefore, to improve the accuracy of the prediction model, the residual stress and strain generated by IC manufacturing process must be taken into consideration shown in Fig. 3.

2 Theory

2.1 Flow analysis theorem

Flow analysis was simulated to get the molding temperature, melting front, velocity, and conversion distribution in the cavity. The governing equations of flow analysis consisted of continuity equation, momentum equation, and energy equation [20].

I. Conservation of mass

$$\frac{\partial \rho}{\partial t} + \nabla \cdot \left(\rho \vec{\mathrm{V}} \right) = 0 \tag{1}$$

ρ, density of EMC; $\vec{v}$, velocity; t, time; ∇, divergence calculator.

II. Conservation of momentum

$$\rho \left(\frac{\partial \vec{\mathrm{V}}}{\partial t} + \vec{\mathrm{V}} \cdot \nabla \vec{\mathrm{V}} \right) = -\nabla \cdot P + \nabla \cdot \vec{\vec{\sigma}} + \rho \vec{\mathrm{g}} \tag{2}$$

∇, gradient; P, pressure; $\vec{g}$, gravity; $\vec{\vec{\sigma}}$, stress tensor.

III. Conservation of energy

$$\rho C_p \left(\frac{\partial T}{\partial t} + \vec{\mathrm{V}} \cdot \nabla T \right) = \nabla \cdot (k \cdot \nabla T) + \eta \dot{\gamma}^2 + \dot{\alpha} \Delta H \tag{3}$$

C_p, specific heat of EMC; T, temperature; k, heat conductivity of EMC; $\dot{\gamma}$, shear rate; ΔH, enthalpy change; $\dot{\alpha}$, cure rate.

2.2 Warpage analysis theorem

EMC material was assumed as linear elasticity, homogeneous, and isotropic. The basic stress–strain relation was expressed by Generalized Hook's law [20]:

$$\{\sigma\} = [D]\left\{\varepsilon^{el}\right\} \tag{4}$$

$\{\sigma\} = \{\sigma_{xx}, \sigma_{yy}, \sigma_{zz}, \sigma_{xy}, \sigma_{yz}, \sigma_{xz}\}^T$, stress matrix; $[D]$, stiffness matrix; $\{\varepsilon^{el}\}$, elastic strain matrix.

For IC packages, warpage and residual stress result from thermal and cure shrinkage. Therefore, elastic strain could be written as:

$$\left\{\varepsilon^{el}\right\} = \left\{\varepsilon^{tot}\right\} - \left(\left\{\varepsilon^{th}\right\} + \left\{\varepsilon^{C}\right\}\right) \tag{5}$$

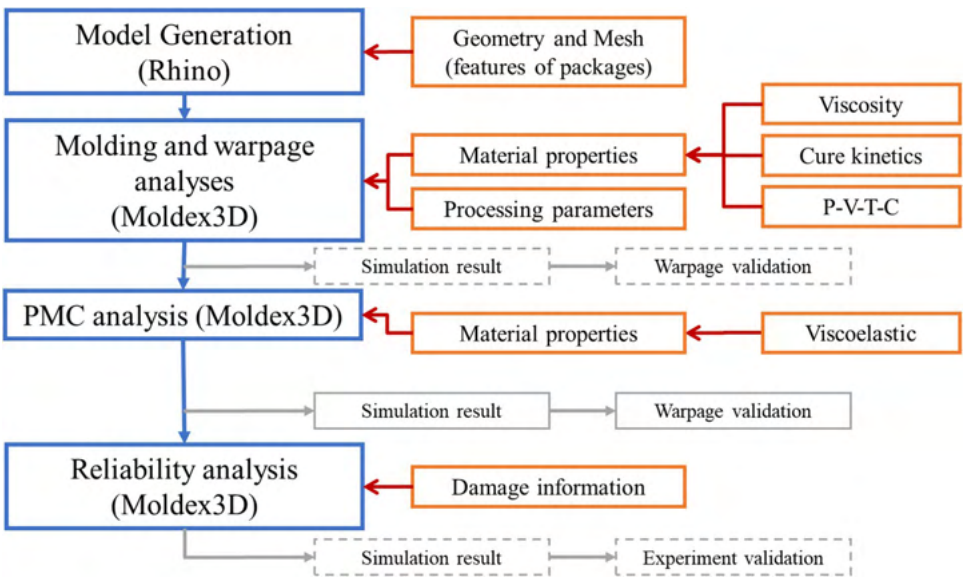

Fig. 3 Analysis procedure of IC package simulation

$\{\varepsilon^{tot}\}$, total strain matrix; $\{\varepsilon^{th}\}$, thermal-induced strain matrix; $\{\varepsilon^{C}\}$, cure-induced strain matrix.

Consequently, total strain can be written as:

$$\left\{\varepsilon^{tot}\right\} = \left\{\varepsilon^{C}\right\} + \left\{\varepsilon^{th}\right\} + \left\{\varepsilon^{el}\right\} = \left\{\varepsilon^{C}\right\} + \alpha\Delta T + [D]^{-1}\{\alpha\} \tag{6}$$

$$[D]^{-1} = \begin{bmatrix} 1/E_{xx} & -\nu_{xy}/E_{xx} & -\nu_{xz}/E_{xx} & & & \\ -\nu_{yx}/E_{yy} & 1/E_{yy} & -\nu_{yz}/E_{yy} & 0 & & \\ -\nu_{zy}/E_{zz} & -\nu_{zy}/E_{zz} & 1/E_{zz} & & & \\ & & & 1/G_{xy} & 0 & 0 \\ & 0 & & 0 & 1/G_{yz} & 0 \\ & & & 0 & 0 & 1/G_{zx} \end{bmatrix} \tag{7}$$

$[D]^{-1}$, inverse matrix of the stiffness matrix; E_{xx}, Young's modulus along x direction; ν_{xy}, Poisson's ratio.

Then, the governing equations of stress–strain relationship were obtained:

$$\varepsilon_x\alpha\Delta T + \varepsilon_C + \frac{\sigma_{xx}}{E_{xx}} - \frac{\nu_{xy}\sigma_{yy}}{E_{xx}} - \frac{\nu_{xy}\sigma_{zz}}{E_{xx}} \tag{8}$$

$$\varepsilon_y = \alpha \triangle T + \varepsilon_C - \frac{V_{xy}\,\delta_{xx}}{E_{yy}} + \frac{\delta_{yy}}{E_{yy}} - \frac{\delta_{zz}}{E_{yy}} \tag{9}$$

$$\varepsilon_{z=}\alpha\Delta T + \varepsilon_C - \frac{\nu_{xz}\sigma_{xx}}{E_{zz}} - \frac{\nu_{yz}\sigma_{yy}}{E_{zz}} + \frac{\sigma_{zz}}{E_{zz}} \tag{10}$$

Assume EMC material is linear viscoelastic, homogeneous, and isotropic as well as load bearings, its stress tensor will be:

$$\vec{\vec{\sigma}} = \begin{bmatrix} \sigma_{xx} & \tau_{xy} & \tau_{xz} \\ \tau_{yx} & \sigma_{yy} & \tau_{yz} \\ \tau_{zx} & \tau_{zy} & \sigma_{zz} \end{bmatrix} = \begin{bmatrix} -P & 0 & 0 \\ 0 & -P & 0 \\ 0 & 0 & -P \end{bmatrix} + \begin{bmatrix} S_{xx} & S_{xy} & S_{xz} \\ S_{yx} & S_{yy} & S_{yz} \\ S_{zx} & S_{zy} & S_{zz} \end{bmatrix} \tag{11}$$

$$-P = \frac{1}{3}\left(\sigma_{xx} + \sigma_{yy} + \sigma_{zz}\right) \tag{12}$$

$$S_{xx} + S_{yy} + S_{zz} = 0 \tag{13}$$

P, mean stress; $[S]$, deviatoric stress.

Similarly, the strain tensor will be:

$$\vec{\vec{\varepsilon}} = \begin{bmatrix} \varepsilon_{xx} & \varepsilon_{xy} & \varepsilon_{xz} \\ \varepsilon_{yx} & \varepsilon_{yy} & \varepsilon_{yz} \\ \varepsilon_{zx} & \varepsilon_{zy} & \varepsilon_{zz} \end{bmatrix} = \begin{bmatrix} \theta & 0 & 0 \\ 0 & \theta & 0 \\ 0 & 0 & \theta \end{bmatrix} + \begin{bmatrix} e_{xx} & e_{xy} & e_{xz} \\ e_{yx} & e_{yy} & e_{yz} \\ e_{zx} & e_{zy} & e_{zz} \end{bmatrix} \tag{14}$$

$$\theta = \frac{1}{3}\left(\varepsilon_{xx} + \varepsilon_{yy} + \varepsilon_{zz}\right) \tag{15}$$

$$e_{xx} + e_{yy} + e_{zz} = 0 \tag{16}$$

θ, mean strain; $[e]$, deviatoric strain tensor.

When a viscoelastic material is load-bearing, its transient relation between stress and strain under time variation can be expressed as

$$\sigma_{ij} = \varepsilon_{kl}(0)R_{\mathrm{ijkl}}(t) + \int_0^t R_{\mathrm{ijkl}}(t-\tau)\frac{\partial\varepsilon_{kl}(\tau)}{\partial\tau}d\tau \tag{17}$$

$R_{ijkl}(t)$, relaxation modulus of the material; $\varepsilon_{kl}(0)$, material strain in the initial state.

Because the material is isotropic and homogeneous, the material relaxation modulus can be rewritten as:

$$R_{\mathrm{ijkl}}(t) = \frac{1}{3}[K(t) - G(t)]\widehat{\sigma}_{ij}\widehat{\sigma}_{kl} + \frac{1}{2}G(t)\left[\widehat{\sigma}_{ik}\widehat{\sigma}_{jl} - \widehat{\sigma}_{il}\widehat{\sigma}_{jk}\right] \tag{18}$$

$K(t)$, volume relaxation modulus; $G(t)$, shear relaxation modulus; σ_{ij}, kronecker delta function.

3 Material model

3.1 Viscosity model

Cross Castro-Macosko model is used for the viscosity calculation of EMC:

$$\eta = \frac{\eta_0\left(\frac{C_g}{C_g - C}\right)^{k_1 + k_2 C}}{1 + \left(\frac{\eta_0\dot{\gamma}}{\tau^*}\right)^{1-n}} \tag{19}$$

$$\eta_0 = A \cdot exp\left(\frac{T_b}{T}\right) \tag{20}$$

C, degree of cure; η, viscosity; η_0, zero-shear-rate viscosity; $\dot{\gamma}$, shear strain rate; τ^*, critical shear stress; n, power law index; C_g, degree of cure at gel point; k_1, k_2, A, T_b, model constants.

The constants of model were seen in Table 1, and the relationship of viscosity and temperature was illustrated in Fig. 4.

Table 1 Viscosity model constants

Model	Parameter	Value	Unit
Cross Castro Macosko model	C_g	0.7	–
	k_1	0.38	–
	k_2	−1.45	–
	A	4.78×10^{-17}	g/(cm-s)
	T_b	19,201	K
	n	0.43	–
	τ^*	100	Dyne/cm^2

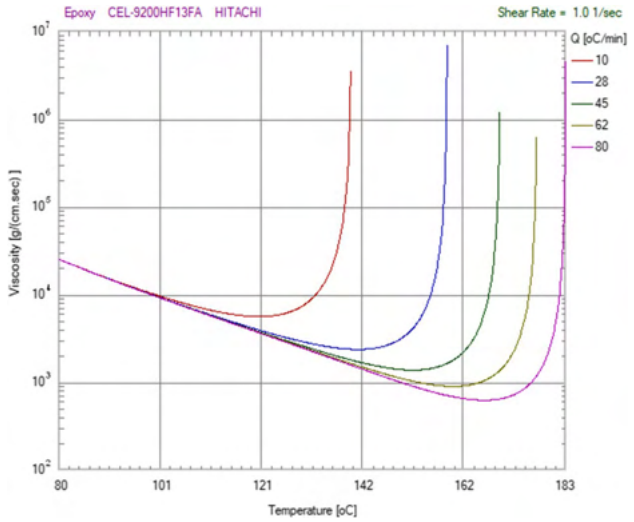

Fig. 4 Viscosity vs. temperature

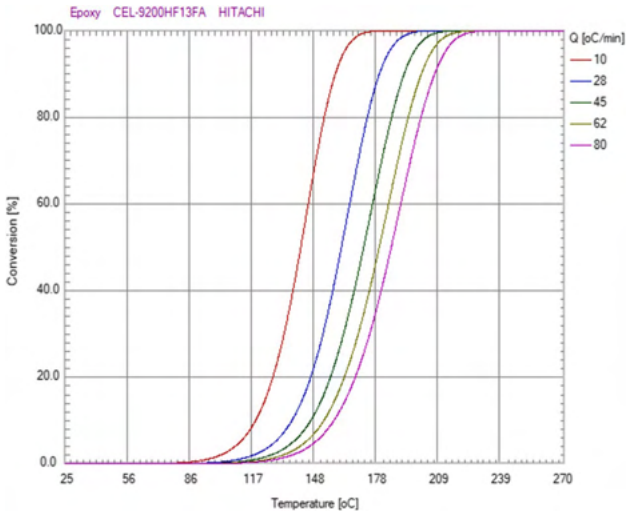

Fig. 5 Conversion vs. temperature

3.2 Cure kinetics model

Kamal's model is used for the cure kinetics calculation of EMC:

$$\dot{C} = \frac{dC}{dt} = \left(K_a + K_b \cdot C^m\right) \cdot (1 - C)^n \tag{21}$$

$$K_a = A \cdot exp\left(-\frac{T_a}{T}\right), K_b = B \cdot exp\left(-\frac{T_b}{T}\right) \tag{22}$$

$\dot{C}$, cure reaction rate; A, B, m, n, K_a, K_b, model constants; E_a, E_b, activation energies; T_a, T_b, activation temperature.

The constants of the model are seen in Table 2, and the relationship of conversion and temperature is illustrated in Fig. 5.

3.3 *P–V-T-C* model

Two-domain modified Tait model is used for the *P–V-T-C* relation of EMC:

Table 2 Cure kinetics model constants

Model	Parameter	Value	Unit
Kamal's model	m	0.38	-
	n	0.86	-
	A	987.17	1/s
	B	67,504	1/s
	T_a	6,364	K
	T_b	6,574	K
	dH	1.83×10^8	erg/g

$$\frac{1}{V} = \frac{1}{V_{\text{uncured}}} \cdot (1 - C) + \frac{1}{V_{\text{cured}}} \cdot C \tag{23}$$

$$V_{\text{uncured}}/V_{\text{cured}} = V_0\left[1 - \alpha \cdot \ln\left(1 + \frac{P}{B}\right)\right] \tag{24}$$

$$V_0 = \begin{cases} b_{1S} + b_{2S}\left(T - b_5\right), \text{if } T \le T_{\text{trans}} \\ b_{1L} + b_{2L}\left(T - b_5\right), \text{if } T > T_{\text{trans}} \end{cases} \tag{25}$$

$$B = \begin{cases} b_{3S} \cdot \exp\left[-b_{4S} \cdot \left(T - b_5\right)\right], \text{ if } T \le T_{\text{trans}} \\ b_{3L} \cdot \exp\left[-b_{4L} \cdot \left(T - b_5\right)\right], \text{ if } T > T_{\text{trans}} \end{cases} \tag{26}$$

$$T_{\text{trans}}\,(P) = b_5 + b_6, \alpha = 0.0894 \tag{27}$$

C, degree of cure; V, specific volume; V_0, specific volume at zero gauge pressure; B, accounts for pressure sensitivity of the material; b_6, linear increase in T_{trans} with pressure; b_5, transition temperature at zero gauge pressure.

The constants of the model are seen in Table 3, and the *P–V-T-C* relationship is illustrated in Fig. 6.

3.4 Viscoelastic model

Dual shift factor model is used for the viscoelastic calculation of EMC:

$$E\,(t) = E_\infty + \sum_{i=1}^{N} E_i \cdot \exp\left(-\frac{t}{\lambda_i}\right) \tag{28}$$

$$\lambda_i\,(T) = \lambda_i\left(T_f\right) \cdot a_T\,(T) \cdot a_C\,(C) \tag{29}$$

Table 3 *P–V-T-C* model constants

Model	Parameter	Value	Unit
Two-domain modified Tait model	b_{1L}	0.5934	cc/g
	b_{2L}	0.00015	cc/(g-K)
	b_{3L}	4.37×10^{9}	dyne/cm^2
	b_{4L}	0.00943	1/K
	b_{1S}	0.593	cc/g
	b_{2S}	6.71×10^{-5}	cc/(g-K)
	b_{3S}	5.31×10^{9}	dyne/cm^2
	b_{4S}	0.005	1/K
	b_5	418.1	K
	b_6	4.49×10^{-9}	(cm^2-K)/dyne

$$a_T = \begin{cases} \exp\left(\frac{-A_1\left(T-T_f\right)}{A_2+\left(T-T_f\right)}\right), \text{ for } T \geq T^* \\ \exp\left(\frac{\Delta H_T}{R}\left(\frac{1}{T}-\frac{1}{T_0}\right)\right), \text{ for } T < T^* \end{cases} \tag{30}$$

$$a_C = \exp\left(\frac{\Delta H_C}{R}\left(\frac{1}{T_g(C)}-\frac{1}{T_{g1}}\right)\right) \tag{31}$$

$$T_g\,(C) = T_{g0} + \frac{\gamma C\left(T_{g1}-T_0\right)}{1-(1-\gamma)C} \tag{32}$$

$E(t)$, stress relaxation modulus; T_f, reference temperature; T^*, critical temperature; A_1, A_2, WLF model constants; $\Delta H_T/R$, $\Delta H_C/R$, active energy; T_g, glass transition temperature.

The constants of the model are seen in Tables 4 and 5, and the relationship of modulus and time is illustrated in Fig. 7.

4 Simulation

For the simulation of IC encapsulation process, Moldex3D can establish a series analysis procedure for IC packages. Through powerful parallel computing functions, complex calculations can be completed in a short time. It does not improve the efficiency of computer calculations because it can bear a larger number of mesh.

Table 4 Viscoelastic model constants

Model	Parameter	Value	Unit
Dual shift factor model	A_1	8.35	-
	A_2	127.25	K
	T_f	393.15	K
	T^*	363.15	K
	T_0	536.78	K
	T_{g0}	323	K
	T_{g1}	387.24	K
	γ	0.127	-
	E_∞	1.54×10^{9}	dyne/cm^2
	$\Delta H_T/R$	13,300	K
	$\Delta H_C/R$	29,141	K

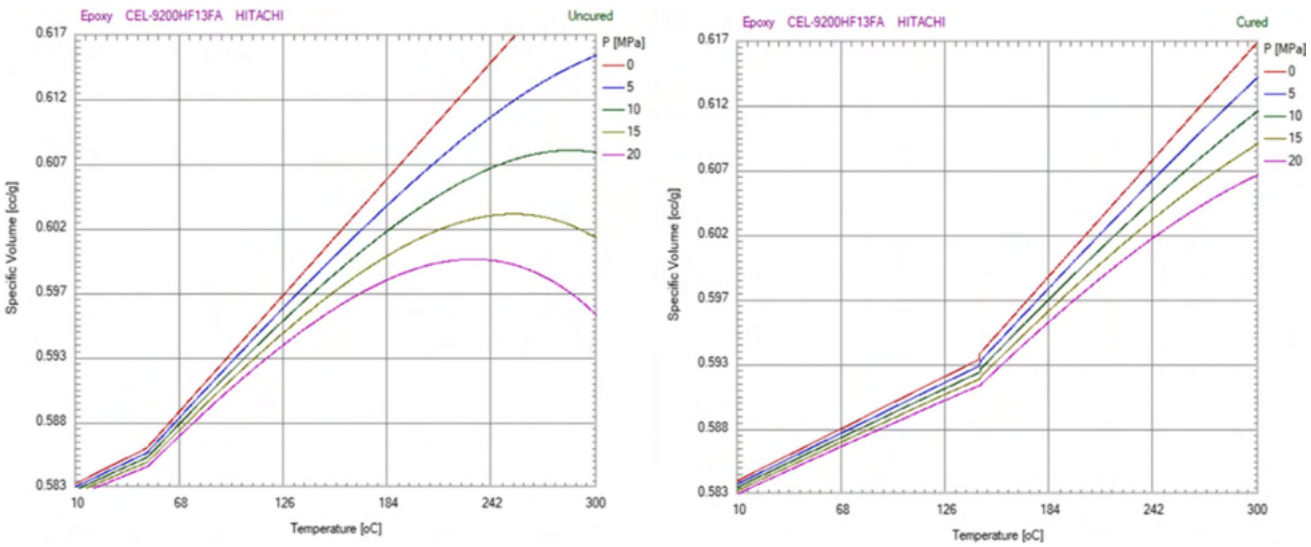

(a) Uncured (b) Cured

Fig. 6 *P–V-T-C* relationship

Table 5 Viscoelastic model parameters

	E (dyne/cm^2)	λ (s)
1	2.90×10^{9}	1.00×10^{-9}
2	3.28×10^{9}	4.64×10^{-8}
3	4.77×10^{9}	2.15×10^{-6}
4	1.18×10^{10}	0.001
5	2.65×10^{10}	0.00464
6	1.81×10^{10}	0.215
7	7.96×10^{9}	10
8	2.92×10^{9}	464
9	1.26×10^{9}	24,500
10	4.69×10^{7}	1.00×10^{6}

4.1 Mesh model and mechanical properties

As shown in Fig. 8, the case was TSOP 48L and supplied by ChipMOS. A unit consists of a lead frame, a tape, a die, wires, and EMC. To simplify the mesh model, tape and wires were ignored shown in Fig. 9.

Table 6 shows the material properties of each component in the IC package.

4.2 Transfer molding analysis

Figure 10 shows the parameter settings of molding process, including mold temperature, material temperature, filling time, filling pressure, curing time, curing pressure, curing switch, and initial conversion. These following parameters were provided by ChipMOS.

In order to observe the deformation trend of the unit, 19 measured nodes are set. There are 9 nodes in the long direction, 5 nodes in the short direction, and 7 nodes in the diagonal direction, as shown in Fig. 11.

Figure 12 shows the simulation results after molding. In general, a fine filling result should show balanced flow contribution of each gate and all flow paths should reach the cavity wall at the same time. When the filling rate reaches 80% and 95%, melting front does not reach cavity wall at the same time because of asymmetry of the lead frame structure.

Figure 13 shows the results after curing process of the unit analysis indicated EMC conversion of approximately 90–95%, which was uncured. Therefore, PMC process must be carried out to make the EMC reach a fully cured state, also improve the mechanical properties and reliability.

The volumetric shrinkage after molding is about 2.2% shown in Fig. 14. When the unit is cooled from high temperature to room temperature after transfer molding, volume shrinkage of EMC is affected by *P–V-T-C* relationship. As shown in Fig. 15, maximum value (− 0.121 mm) is calculated by two-domain modified Tait model.

4.3 PMC analysis

Figure 16 and Table 7 show the environment condition for PMC process. The unit is placed in an oven at a temperature of 175 °C for 4 h to make package to be fully cured. Viscoelastic behavior and gravity are also considered. The convection coefficient is 25 W/m^2-K.

Figures 17 and 18 are the schematic figures simulated the sample always pressed on the board with 0.04 MPa. It is noted that the pressure is only applied at 175 °C, which is from the 200th second to 14180th second.

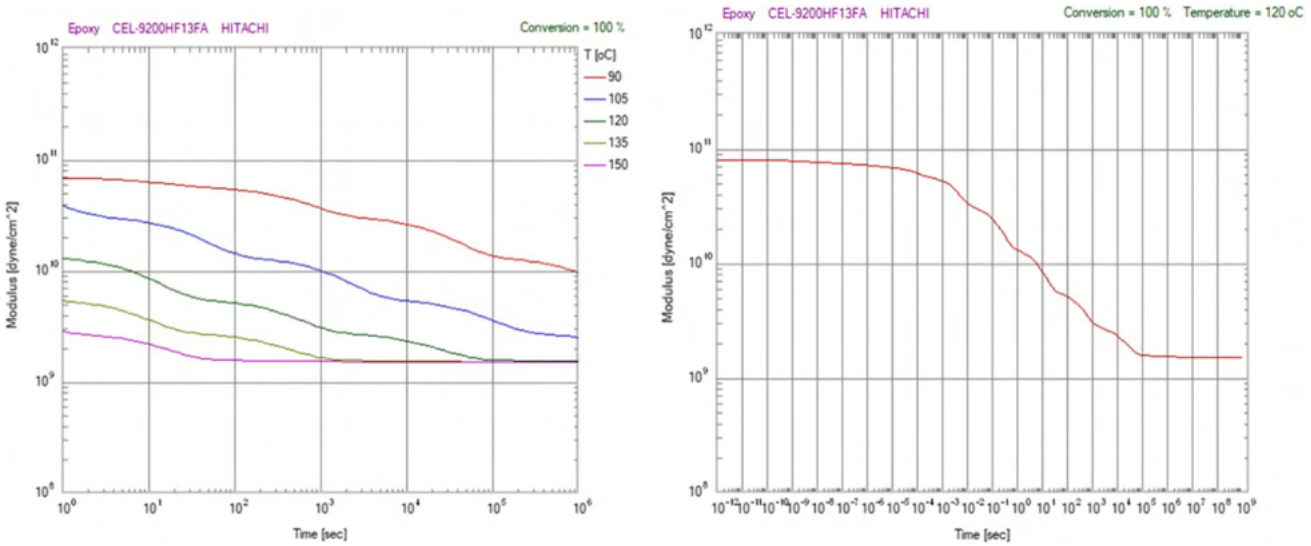

Fig. 7 Master curve of the relaxation modulus

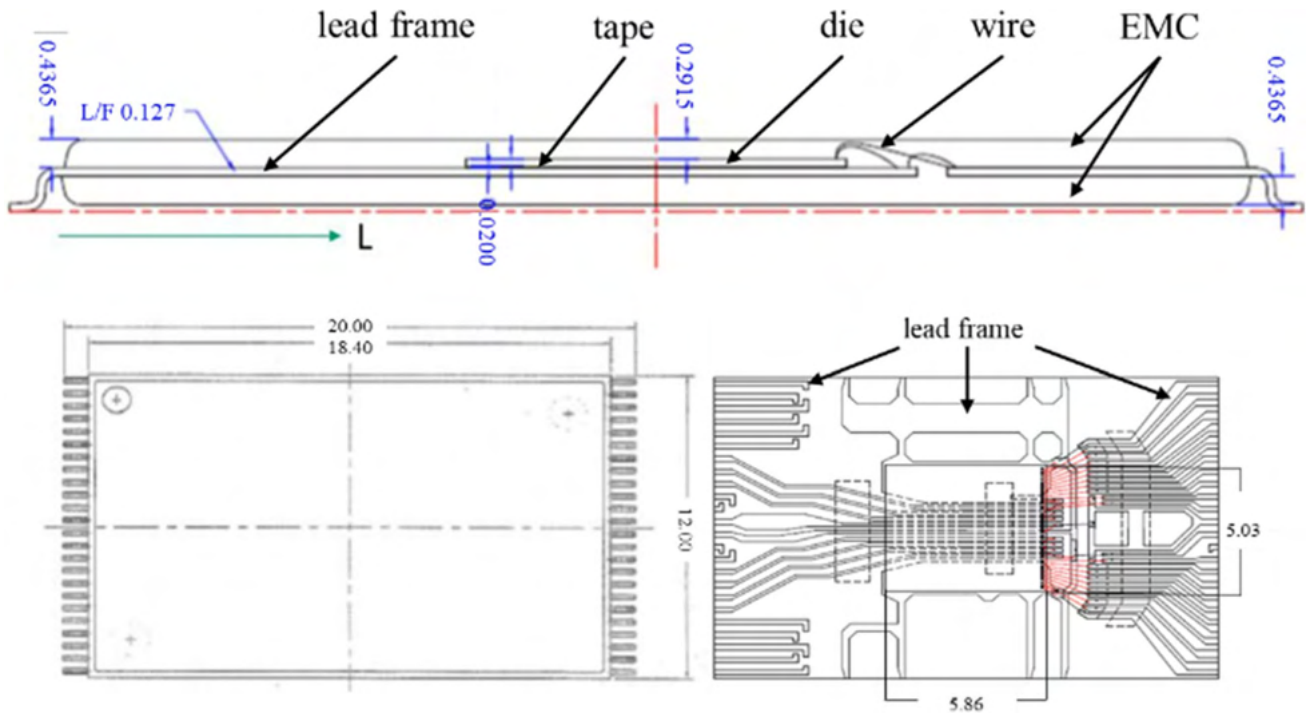

Fig. 8 Geometry of TSOP unit

Fig. 9 Mesh model of a unit

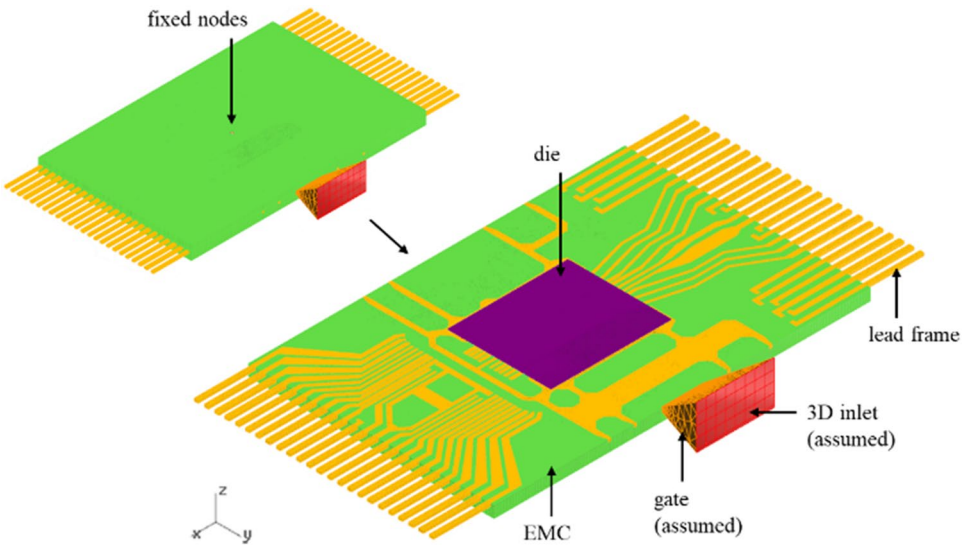

Observe the curing results of PMC analysis as shown in Fig. 19. The conversion of EMC is fully cured after PMC process. It is noted that at 400th second of PMC process, the analysis result shows the conversion of EMC has reached 100%. Subsequently, the effect on warpage of PMC time will be discussed.

After PMC process, shows the unit deformed due to the long-term viscoelastic behavior of EMC. The deformation trend is asymmetrical and concave downward. Maximum value (− 0.119 mm) of warpage is calculated by the dual shift factor model (Fig. 20).

Figure 21 shows the deviations between experiments and simulations. There is about 5–30% error in the long direction, 40–50% error in the short direction, and 10–30% error in the diagonal direction.

Next, the PMC time and PMC temperature will be changed individually to discuss how these factors affect the warpage simulation results.

Table 6 Mechanical properties of each component

Component	EMC	Die	Lead frame
Material	9200 HF	Si	Alloy 42
CTE (ppm/°C)	8 35	2.8	4.5
Young's modulus (GPa)	2.60×10^{1}	1.57×10^{2}	1.20×10^{2}
Poisson's ratio	0.2	0.3	0.32
Density (g/cm^3)	2.02	2.33	8.11
Specific heat (J/kg-K)	800	702	200
Thermal conductivity (W/m–K)	1	124	10.5
T_g (°C)	125	-	-

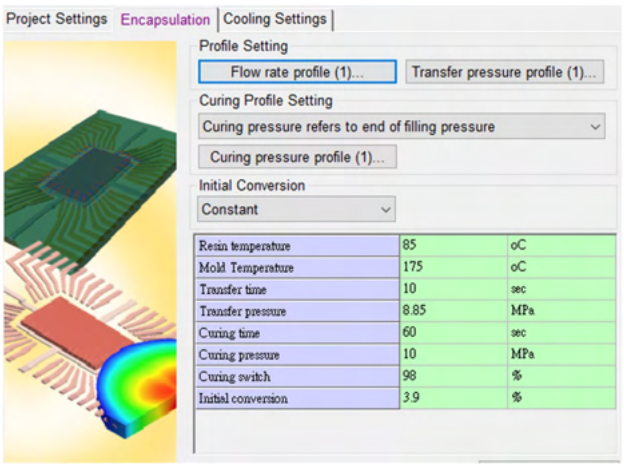

Fig. 10 Molding condition settings

4.4 Effect of PMC time

In the previous PMC simulation, EMC has reached 100% conversion at 400th second. If EMC does not require 4 h of baking to achieve fully cured, the baking time is shortened to 1 h shown in Table 8.

Figure 22 shows the PMC time of 1 h and 4 h have no obvious influence on the warpage results, and the warpage amount is a micron-level variation range.

4.5 Effect of PMC temperature

Since the residual stress induced by the PMC process can affect the reliability prediction (Section 5.1), this section discusses whether the PMC temperature affects the residual stress, while observing the changes in the full curing time and warpage (Table 9). This section discusses three different PMC temperatures, which are 165 °C, 175 °C, and 185 °C, respectively. The actual condition of the PMC process is 175 °C.

4.5.1 Full curing time

The curing time decreases with increasing temperature, in order to clearly understand the effect of temperature on the time required for full curing, The PMC temperature of 165 °C and 185 °C were simulated. The conversion result of PMC temperature at 175 °C is shown in Fig. 19.

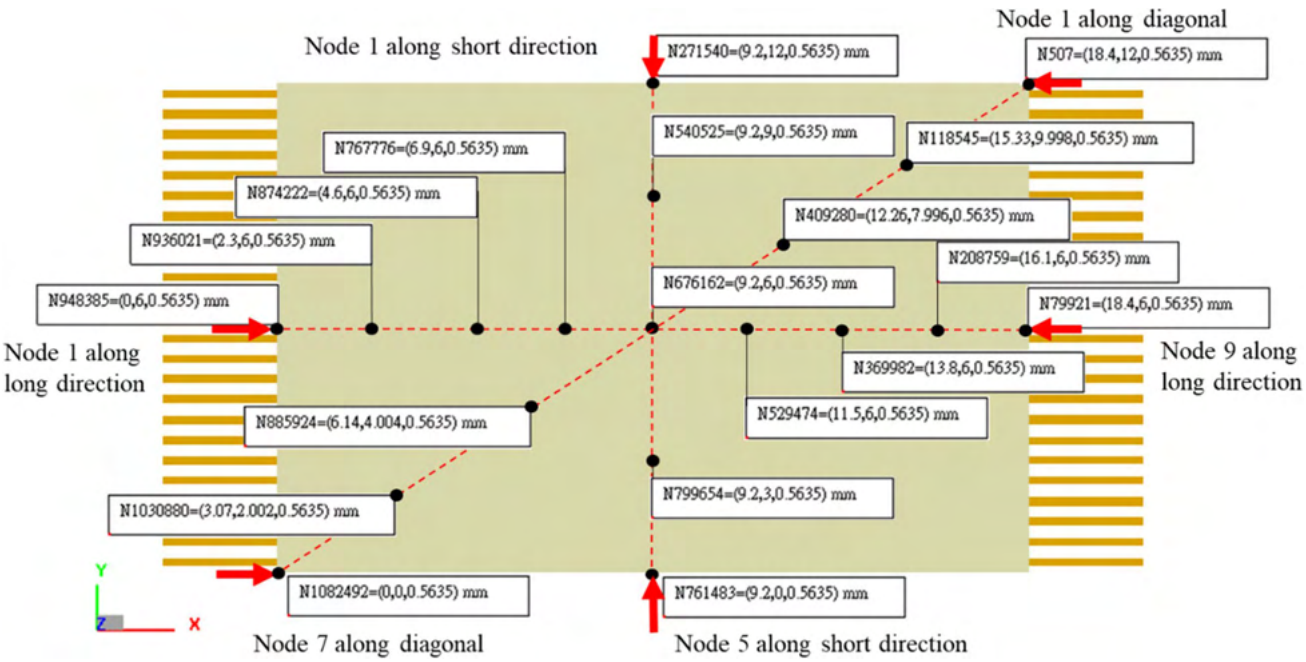

Fig. 11 Measured nodes

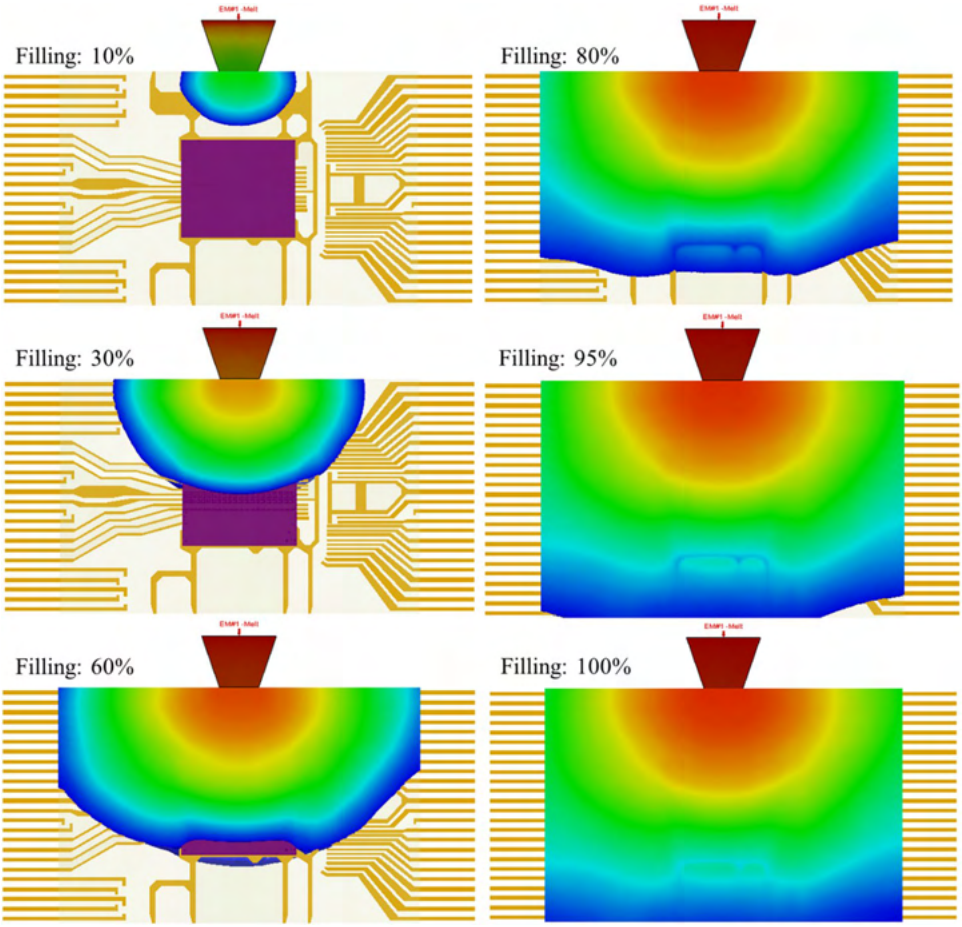

Fig. 12 Melting front results

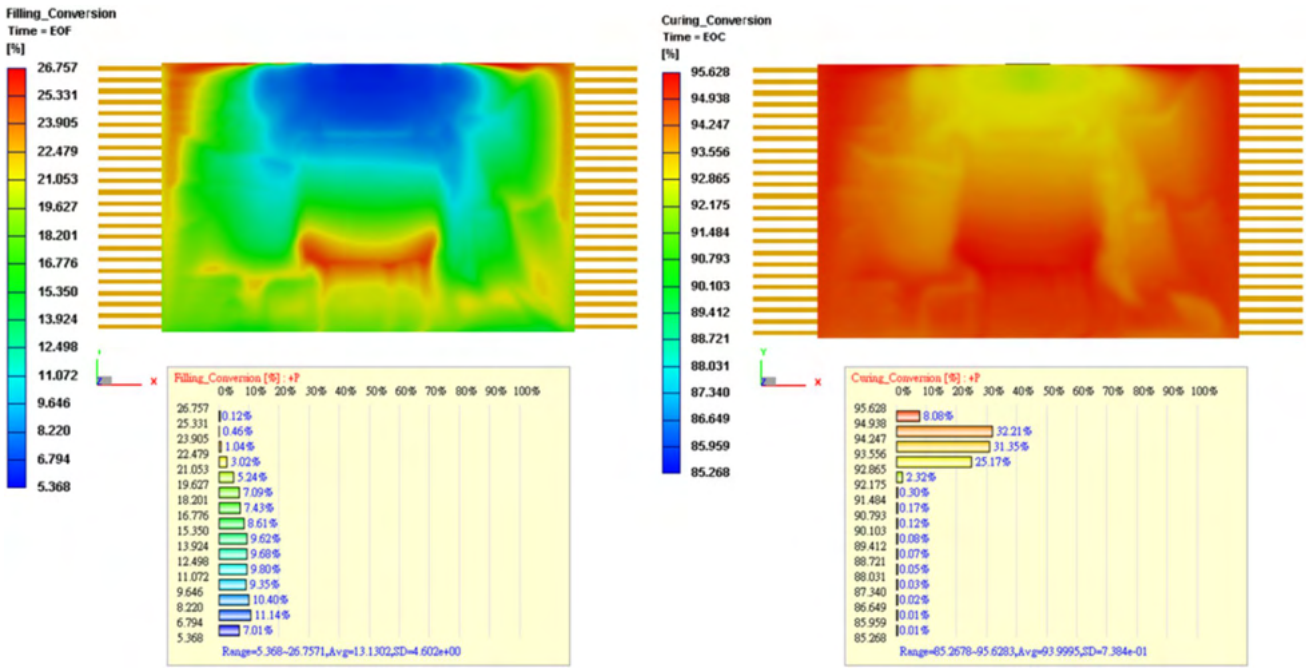

(a) Filling section (b) Curing section

Fig. 13 Degree of cure

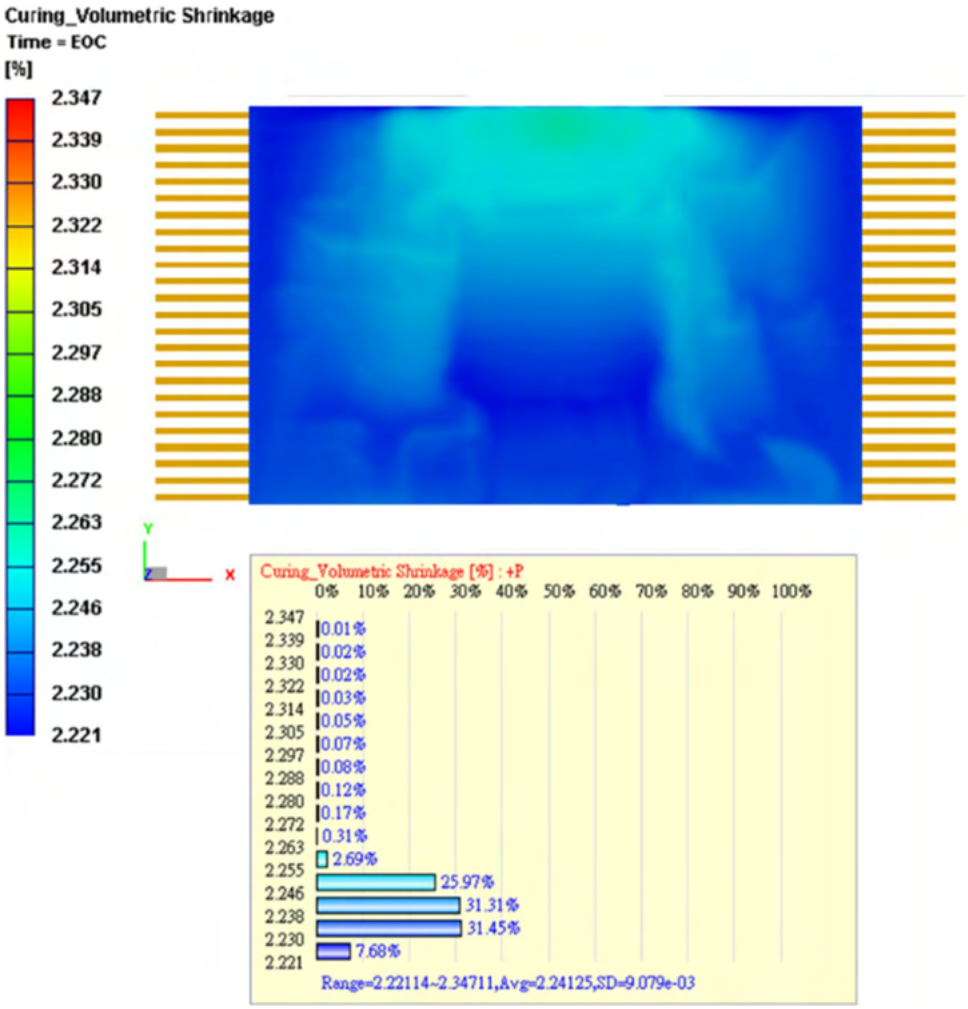

Fig. 14 Volume shrinkage after molding

Figure 23 shows the full curing time of PMC temperature at 165 °C. It can be seen that the full curing time at 500 s after beginning of the PMC process.

Figure 24 shows the full curing time of PMC temperature at 185 °C. It can be seen that the full curing time at 350 s after beginning of the PMC process.

4.5.2 Warpage

The deformation trends of 165 °C PMC temperature and 185 °C PMC temperature is similar to 175 °C PMC temperature.

When the PMC temperature was set to be 165 °C, the maximum warpage is 0.112 mm, and it can be seen in Fig. 25.

When the PMC temperature was set to be 185 °C, the maximum warpage is 0.119 mm, and it can be seen in Fig. 26.

It can be found that when the PMC temperature was set to 165 °C or 185 °C, the change of warpage value is not obvious.

4.5.3 Residual stress

In order to understand the residual stress will be affected by temperature or not, the residual stress simulation is necessary. According to Section 5.1, the lead frame is the possible location of the failure. Here will discuss the PMC process-induced residual stress of the lead frame with 165 °C PMC temperature and 185 °C PMC temperature.

Figure 27 shows PMC process induced residual stress with 165 °C PMC temperature, it can be seen that the maximum Von Mises stress value is 443.92 MPa.

Figure 28 shows PMC process induced residual stress with 185 °C PMC temperature, it can be seen that the maximum Von Mises stress value is 448.34 MPa.

When the PMC temperature change to 165 °C and 185 °C, the PMC process-induced residual stress reduce 7 MPa and 2 MPa. It can be found that the Von Mises stress after the PMC process has a 1.5% variation, changing the PMC temperature has little effect on residual stress.

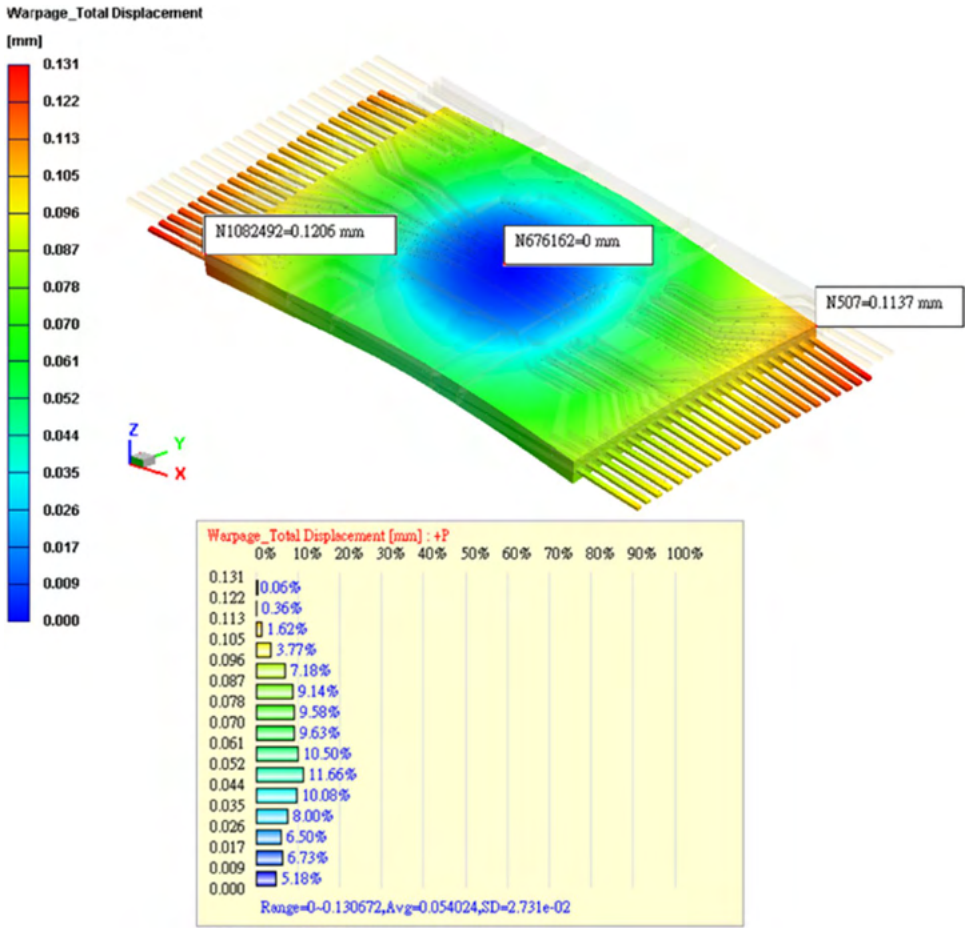

Fig. 15 Warpage after molding

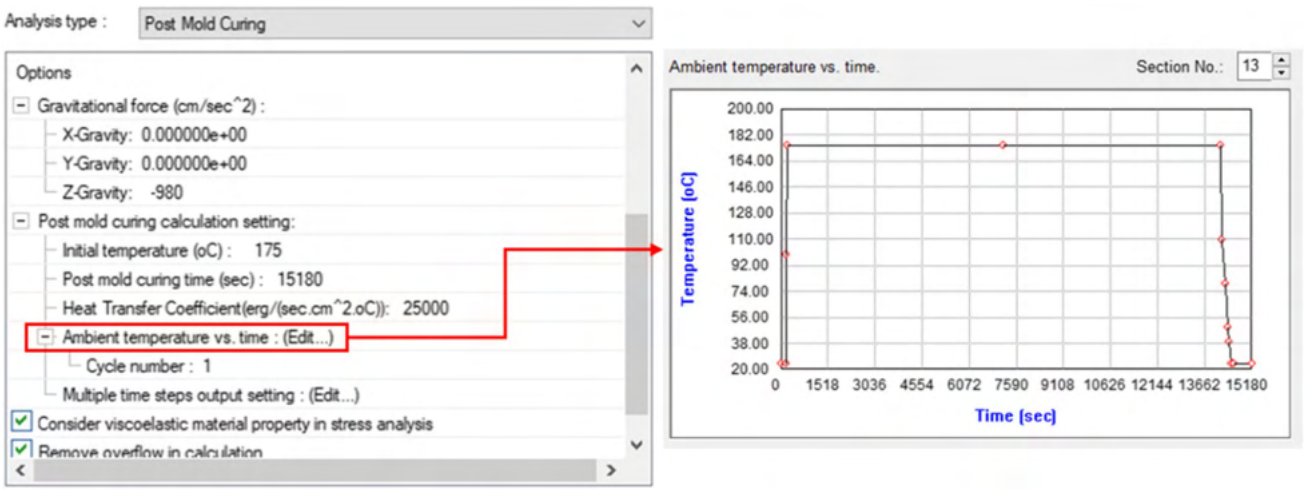

Fig. 16 PMC ambient condition settings

Table 7 PMC temperature condition settings

Time (s)		Temperature (°C)	Time (s)	Temperature (°C)
0		25	14,220	110
180		25	14,340	80
190		100	14,440	50
Loading applied	200	175	14,460	40
	7,180	175	14,520	25
	14,180	175	14,620	25
			15,180	25

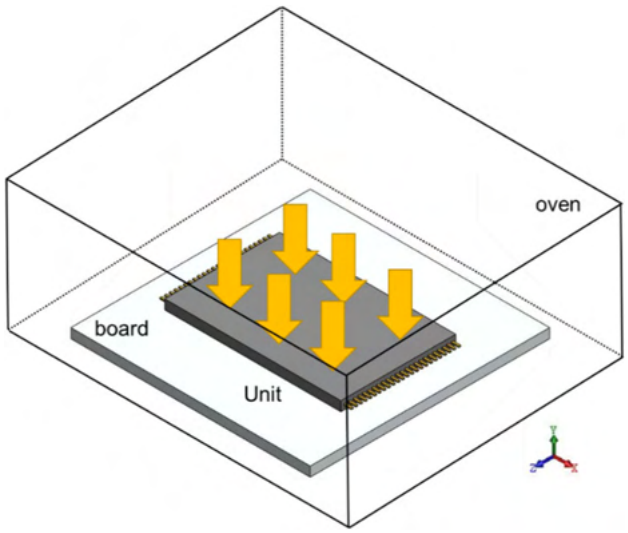

Fig. 17 Loading schematic

5 Thermal analysis

5.1 Thermal cycle

Refer to JEDEC specification [21] for temperature cycle conditions. After the end of PMC, the temperature drops from 25 to − 65 °C in 2 min. And the first thermal cycle starts: temperature rises from − 65 to 150 °C within 5 min and hold the temperature for 15 min; temperature reduces from 150 to − 65 °C within 6 min and hold the temperature for 15 min. As shown in Fig. 29, every cycle is 41 min.

It can be seen from Fig. 30 that after two thermal cycles, the maximum von Mises stress occurs on the die: 778 MPa, which is far from the yield stress of Si: 7 GPa [22].

Observe the Von Mises results of lead frame. The focused place is at the circle location of the figures, where the maximum stress and assumed the firstly damage occurs. The types of damage that occurs accidently may be fatigue cracks, delamination.

From Fig. 31, it can be found that since thermal cycle simulation is performed after PMC simulation, there will be initial stress (450.8 MPa), which is the residual stress after PMC. Figure 32 shows the stress distribution of the lead frame after two temperature cycles. Its von Mises stress is 505.7 MPa. The value is close to the yield stress of lead frame material Alloy 42 of 634 MPa.

At maximum Von Mises stress location where failure can occur, it was found maximum stress value of 730 MPa, minimum stress value of 80 MPa, and mean stress of 405 MPa during thermal cycling, as shown in Fig. 33a. When the process induced residual stress of the PMC process was not taken into account, the initial stress was assumed to be 0 at 25 °C, it was found maximum stress value of 279 MPa, minimum stress value of − 370 MPa, and the mean stress decreased

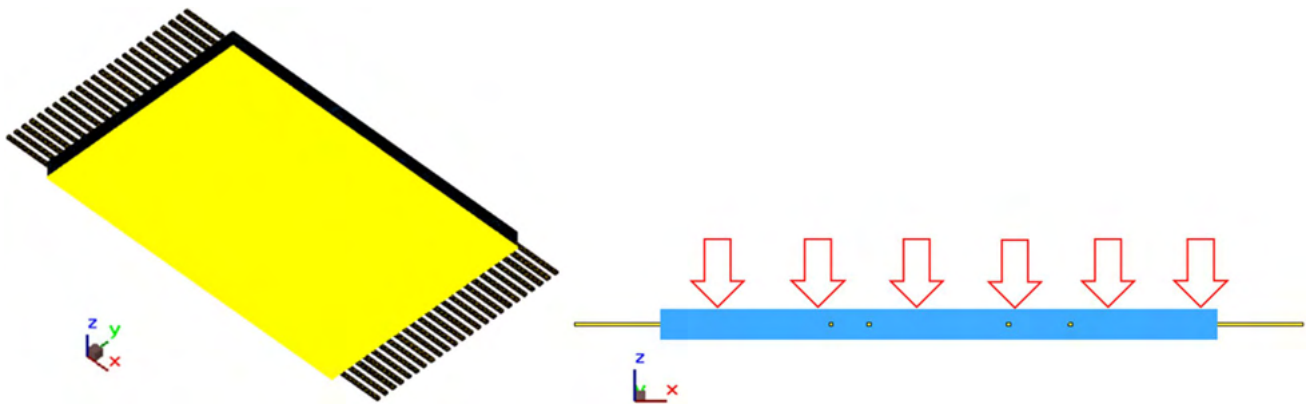

Fig. 18 Boundary condition settings of PMC

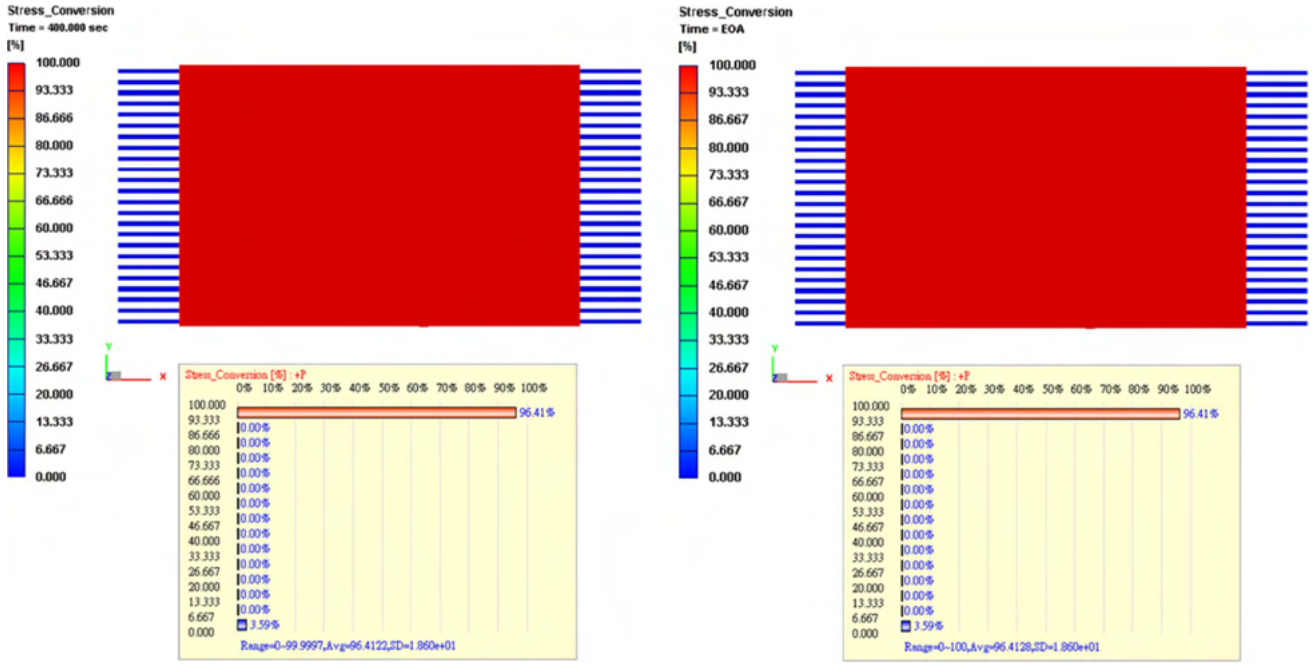

(a) 400th second (b) 15180th second

Fig. 19 Conversion results of PMC

to − 46 MPa. It can be found that stress states are very different when considering or not considering process induced residual stress. It is believed that the prediction of reliability will be strongly affected by the process induced residual stress since its value can be significant.

6 Conclusion

As shown in Table 10, Moldex3D and mathematical model of EMC were used to discuss in detail warpage and residual stress caused by temperature effect and cure effect in molding and PMC processes of IC packages. And use the residual stress results of PMC simulation as the initial condition to analyze reliability of thermal cycles.

In the molding analysis, Cross Castro-Macosko model was used to describe the viscosity of EMC, and Kamal's model was used to describe the cure kinetics of EMC, and two domain-modified Tait model was used to describe the *P–V-T-C* relation. In PMC analysis, dual shift factor model was used to describe viscoelastic properties of EMC. Comparing simulation results with experiment results, the prediction of the trend is correct. The amount of warping has an error of about 5–50%.

Regarding the effect of PMC on warpage, little differences were observed for different PMC duration and PMC temperature conditions. In addition, changing the PMC temperature has little effect on the residual stress. There is only a 1.5% variation in von Mises stress when changing the PMC process temperature. The stress states are very different when considering or not considering process induced residual stress. Taking into account the residual stress induced by the post-mold curing process will make the estimation of package reliability more reasonable.

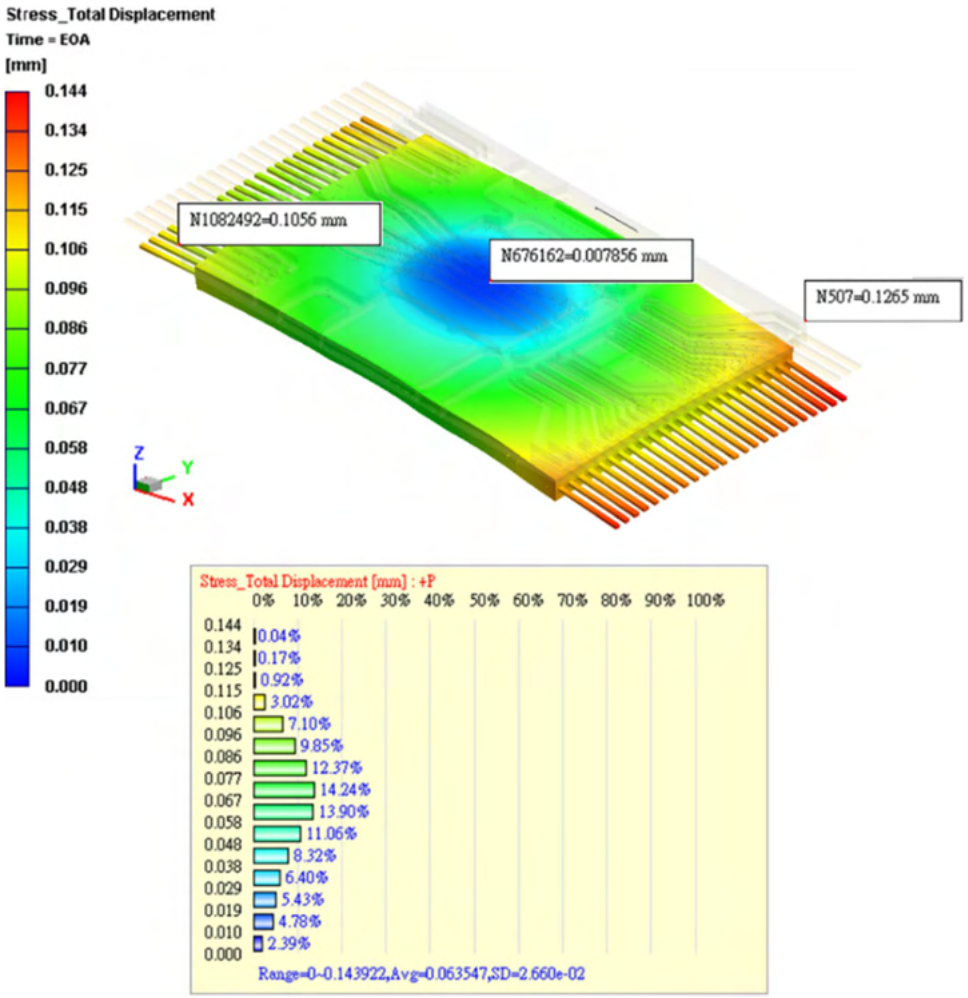

Fig. 20 Warpage results of PMC simulation

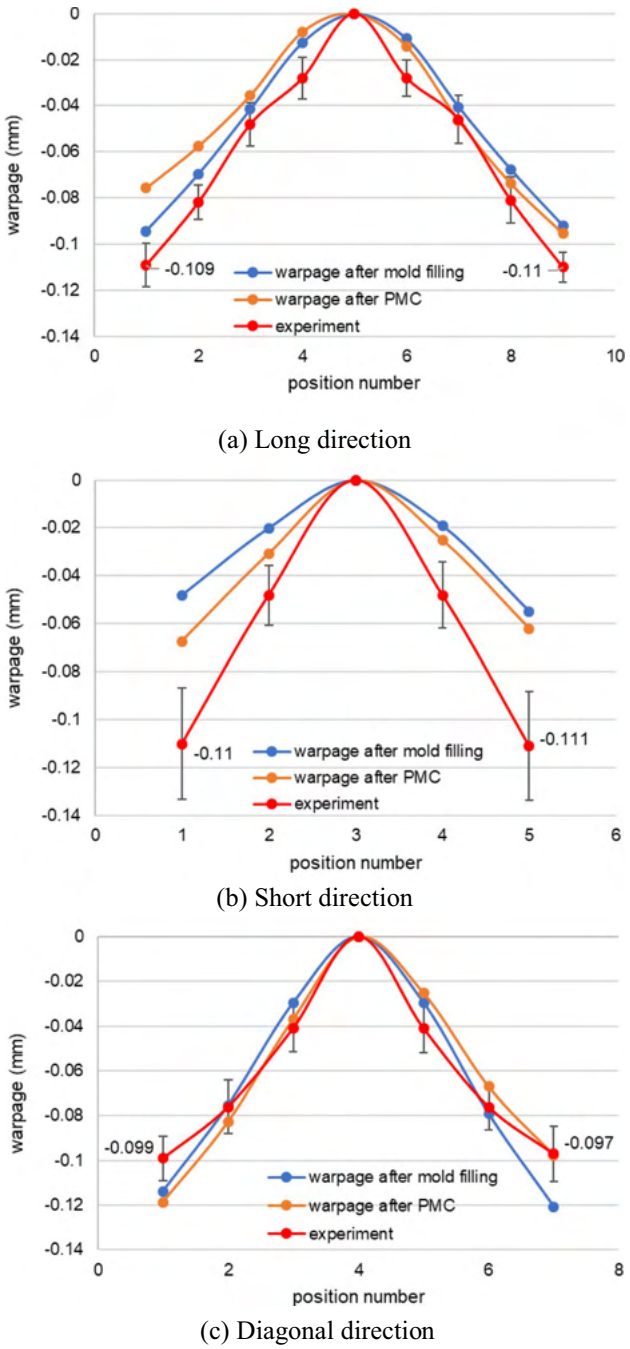

Fig. 21 Warpage comparison of three directions

Table 8 One-hour PMC time of temperature settings

Time (s)		Temperature (°C)	Time (s)	Temperature (°C)
0		25	3840	110
180		25	3900	80
190		100	4020	50
Loading applied	200	175	4080	40
	1000	175	4140	25
	3800	175	4240	25
			4400	25

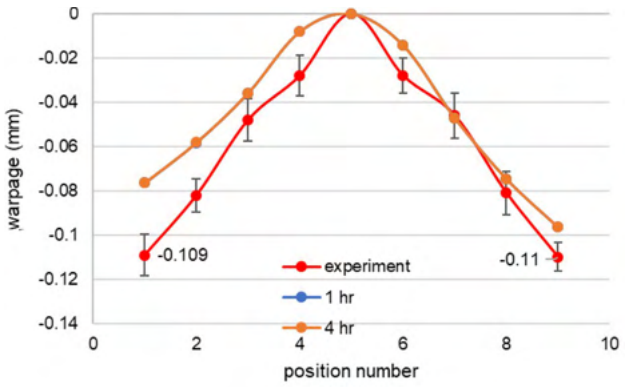

(a) Long direction

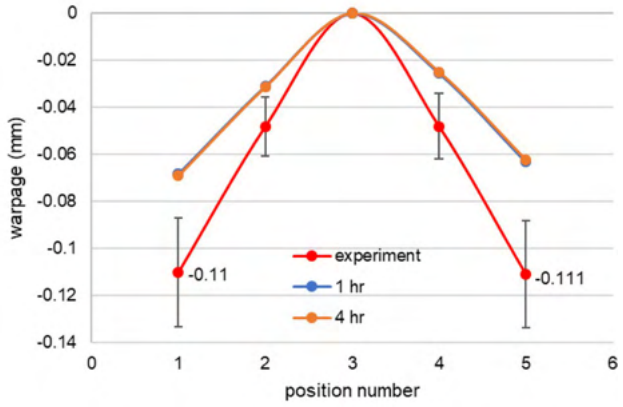

(b) Short direction

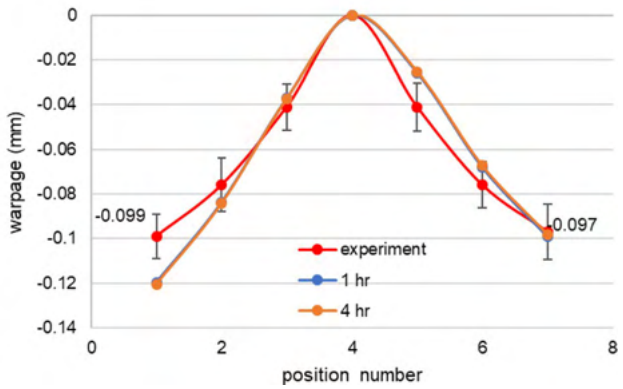

(c) Diagonal direction

Fig. 22 Effect of PMC time

Table 9 Comparing the effect of three PMC temperatures on the package

PMC temperature	165 °C	175 °C	185 °C
Full curing time	500 s	400 s	360 s
Warpage	0.112 mm	0.119 mm	0.119 mm
Maximum von Mises stress of lead frame	443.92 MPa	450.81 MPa	448.34 MPa

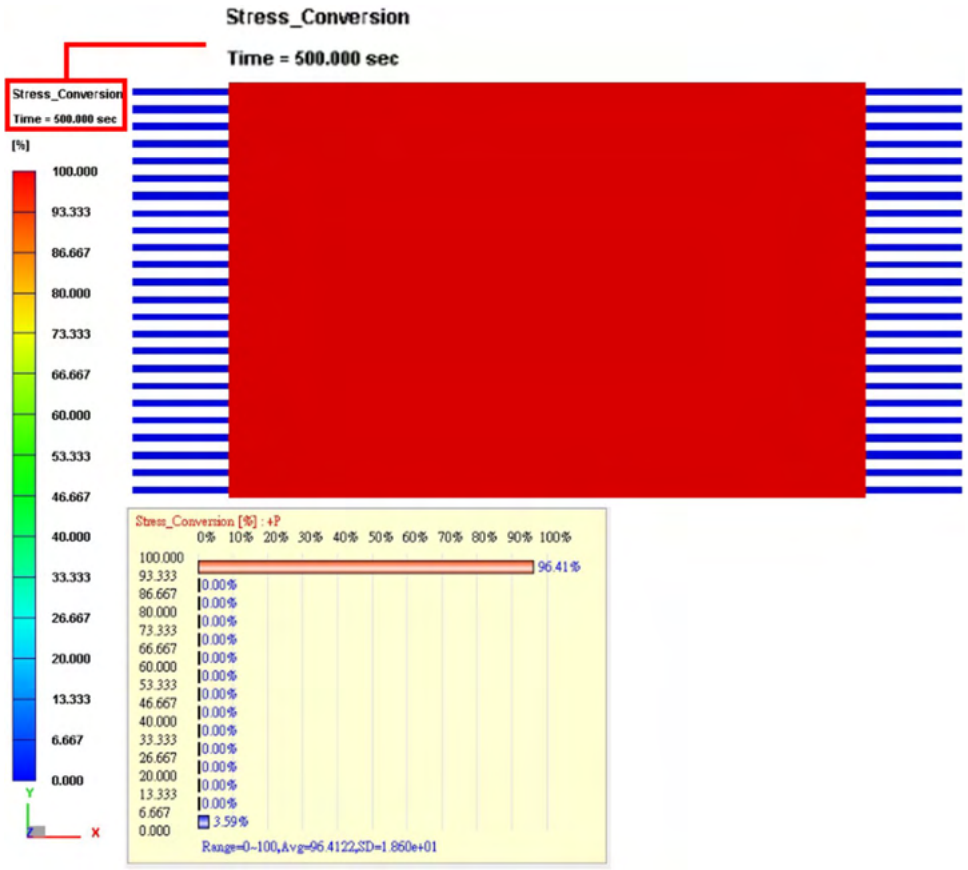

Fig. 23 Full curing time of PMC temperature at 165 °C

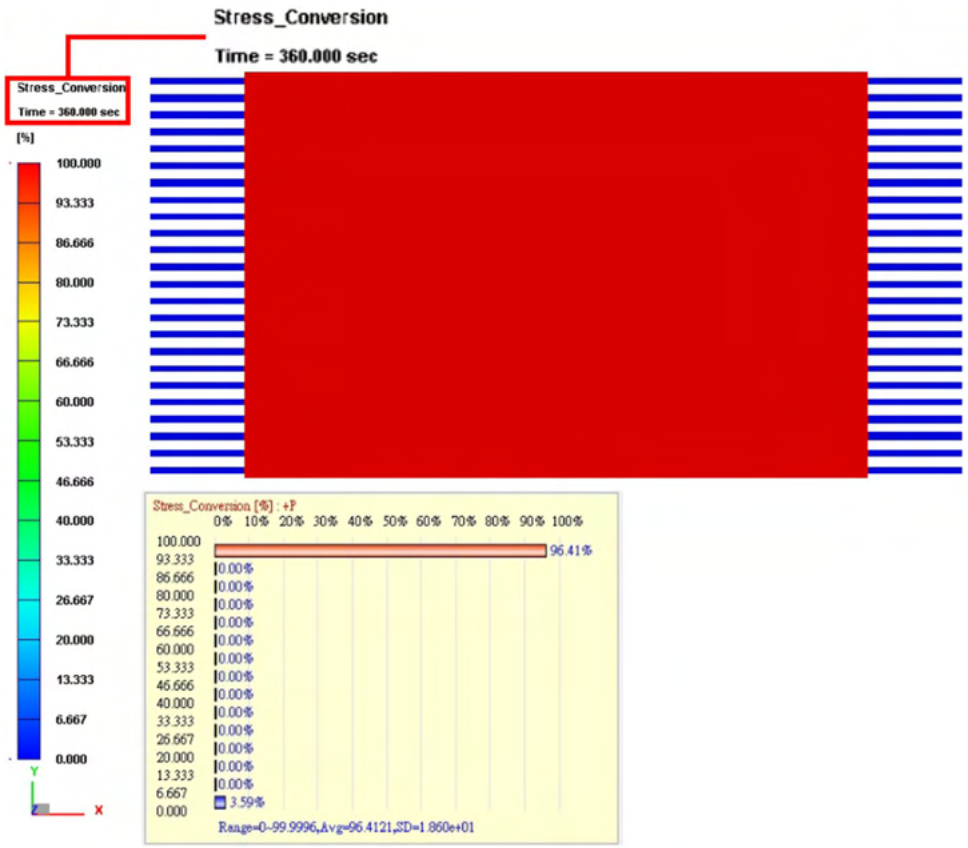

Fig. 24 Full curing time of PMC temperature at 185 °C

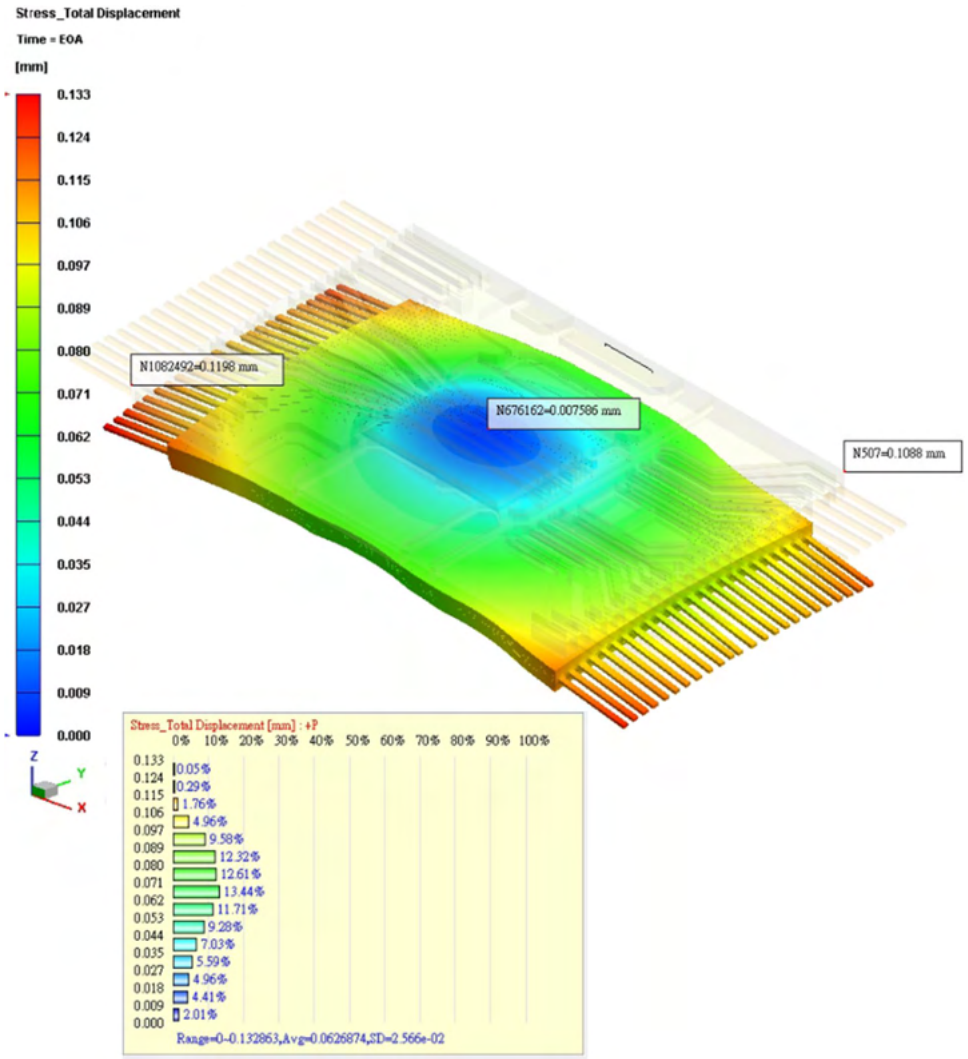

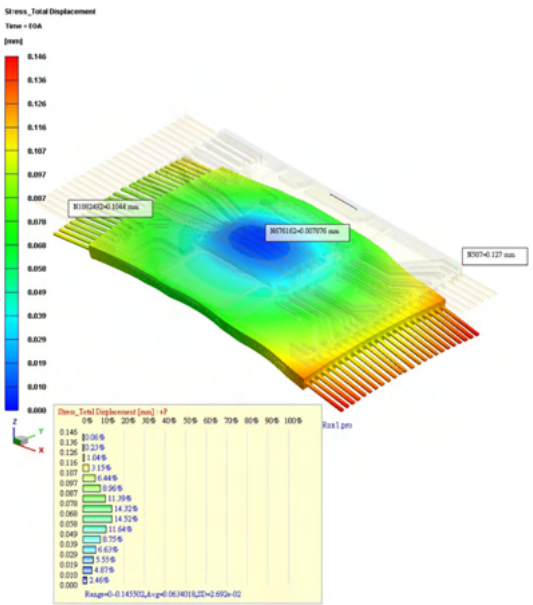

Fig. 25 Warpage results with 165 °C PMC temperature

Fig. 26 Warpage results with 185 °C PMC temperature

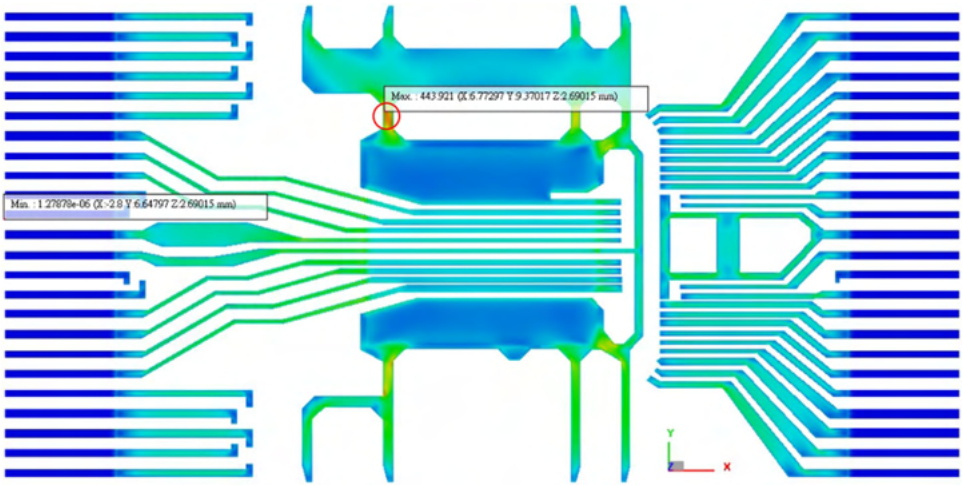

Fig. 27 Von Mises stress after 165 °C PMC process

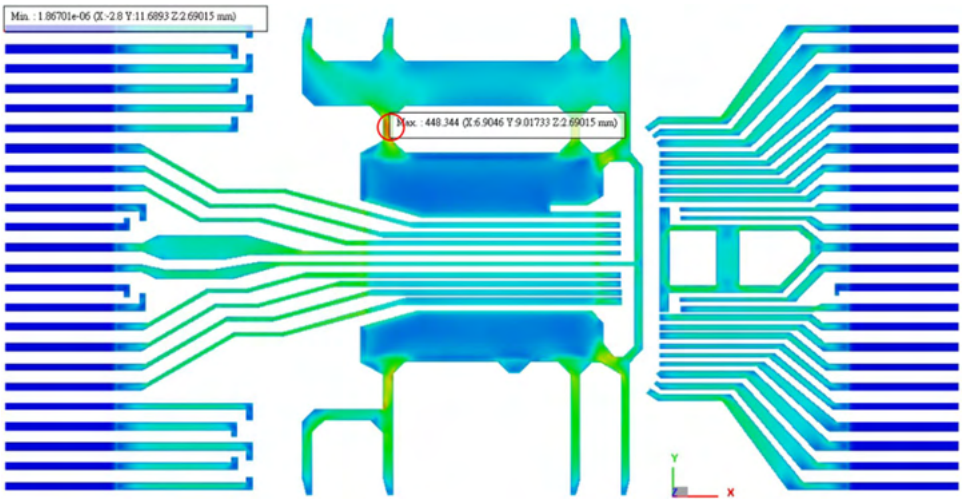

Fig. 28 Von Mises stress after 185˚C PMC process

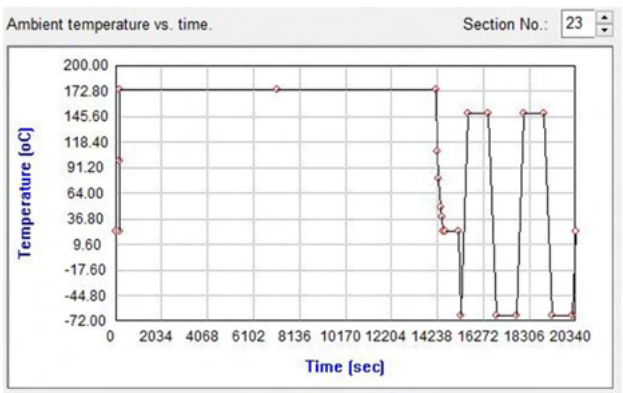

Fig. 29 Temperature profile

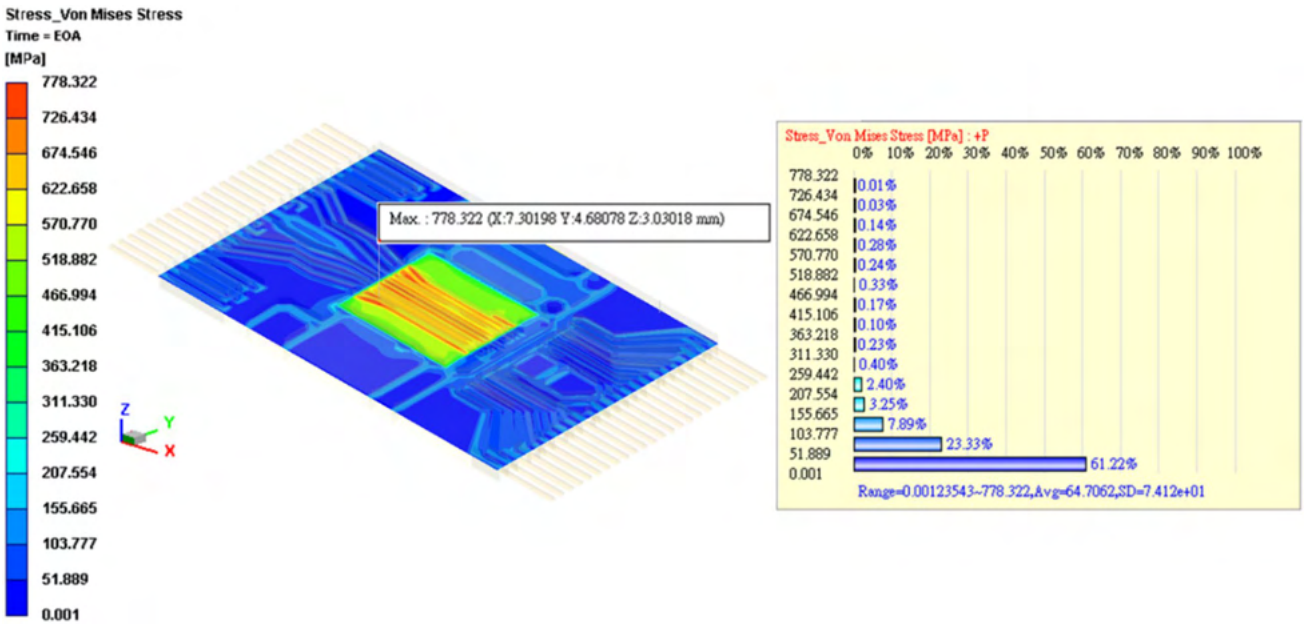

Fig. 30 Von Mises stress result after thermal cycles (Z height: 0.167 mm)

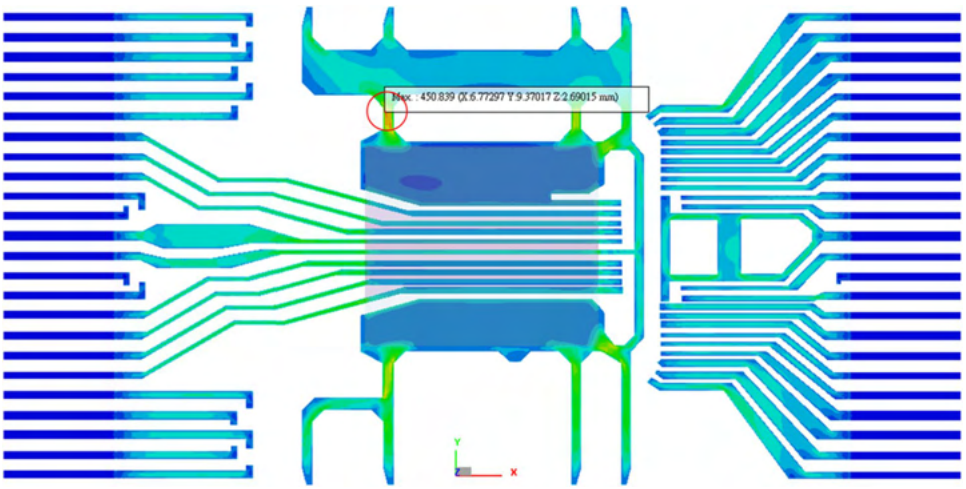

Fig. 31 Von Mises stress distribution after PMC

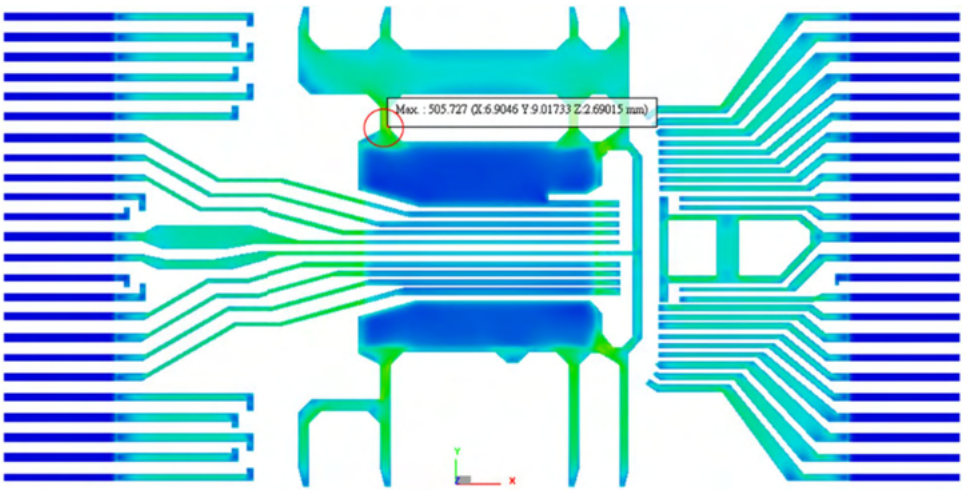

Fig. 32 Von Mises stress distribution after thermal cycles

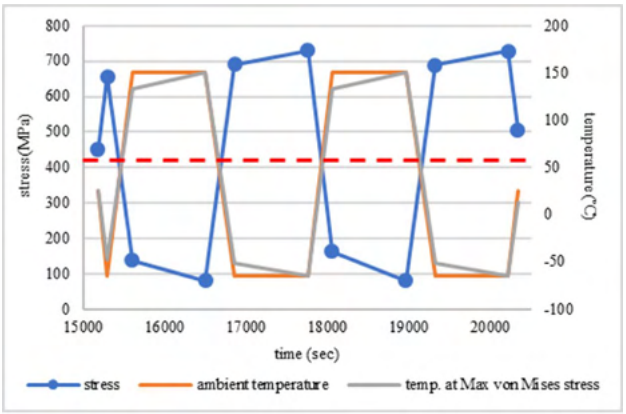

(a) Considering residual stress

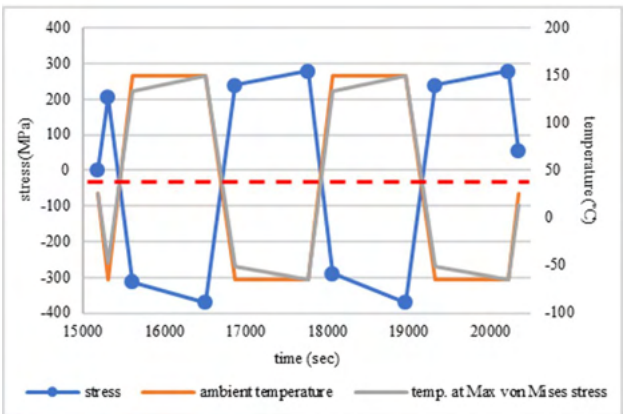

(b) Not considering residual stress

Fig. 33 Von Mises stress vs. time vs. temperature

Table 10 Properties considered in each process analysis

Parameters	Process		
	Filling/curing	PMC	Thermal cycle
Cure kinetics	Y	Y	Y
Viscosity	Y	N	N
P–V-T-C	Y	Y	Y
Viscoelastic	N	Y	Y
Modulus, Poisson ratio	N	Y	Y

Author contribution All authors contributed to the study conception and design. Material preparation, data collection and analysis were performed by Ming-Yu Lin, Ming-Han Wang, Hui-Ping Liu, Chin-Lung Fang, and Sheng-Jye Hwang. The first draft of the manuscript was written by Yong-Jie Zeng, and all authors commented on previous version of the manuscript. All authors read and approved the final manuscript.

Data availability Not applicable.

Code availability Not applicable.

Declarations

Ethics approval The authors confirm the novelty of the reported work and confirm that it is not submitted to any other journal.

Consent for participate The authors give consent to participate.

Consent for publication The authors give consent for publication.

Conflict of interest The authors declare no competing interests.

Open Access This article is licensed under a Creative Commons Attribution 4.0 International License, which permits use, sharing, adaptation, distribution and reproduction in any medium or format, as long as you give appropriate credit to the original author(s) and the source, provide a link to the Creative Commons licence, and indicate if changes were made. The images or other third party material in this article are included in the article's Creative Commons licence, unless indicated otherwise in a credit line to the material. If material is not included in the article's Creative Commons licence and your intended use is not permitted by statutory regulation or exceeds the permitted use, you will need to obtain permission directly from the copyright holder. To view a copy of this licence, visit http://creativecommons.org/licenses/by/4.0/.

References

1. Kelly G, Lyden C, Lawton W, Barrett J (1999) Accurate prediction of PQFP warpage. In: The simulation of thermomechanically induced stress in plastic encapsulated IC packages. Boston, pp 69–85
2. Kelly G, Lyden C, Lawton W, Barrett J, Saboui A, Page H, Peters JB (1996) Importance of molding compound chemical shrinkage in the stress and warpage analysis of PQFP's. IEEE Trans Compon Packag Technol 19:296–300
3. Chang Y-S, Hwang S-J, Lee H-H, Huang DY (2002) Study of P-V-T-C relation of EMC. J Electron Packag 124:371–373
4. Hwang S-J, Chang Y-S (2005) Isobaric cure shrinkage behaviors of epoxy molding compound in isothermal state. J Polym Sci, Part B: Polym Phys 43:2392–2398
5. Hong L-C, Hwang S-J (2004) Study of warpage due to P-V-T-C relation of EMC in IC packaging. IEEE Trans Compon Packag Technol 27:291–295
6. Teng S-Y, Hwang S-J (2007) Simulations of process-induced warpage during IC encapsulation process. J Electron Packag 129:307–315
7. Deng S-S, Hwang S-J, Lee H-H (2013) Warpage prediction and experiments of fan-out waferlevel package during encapsulation process. IEEE Trans Compon Packag Manuf Technol 3:452–458
8. Wang Z-G (2006) Modeling the viscoelastic properties of epoxy molding compound during post mold cure in IC packaging, Master Thesis, Department of Mechanical Engineering, National Cheng Kung University
9. Lin YJ, Hwang S-J, Lee H-H, Huang DY (2011) Modeling of viscoelastic behavior of an epoxy molding compound during and after curing. IEEE Trans Compon Packag Manuf Technol 1:1755–1760
10. Wang JA, Eu OK, Weng WH, Hsu CC, Loh WK, Kulterman RW, Fu H (2020) "Predictive modelling methodologies for bi-material strip warpage." Proceedings of 15th International Microsystems, Packaging, Assembly and Circuits Technology Conference, Taipei, Taiwan
11. Guo H-Y (2020) Prediction of warpage considering *P-V-T-C* relation and viscoelastic behavior of EMC during IC encapsulation process. Master Thesis, Department of Mechanical Engineering, National Cheng Kung University
12. Coffin LF (1954) A study of the effects of cyclic thermal stresses on a ductile metal. Trans ASME 76:931–950
13. Shi XQ, Pang HLJ, Zhou W, Wang ZP (2000) Low cycle fatigue analysis of temperature and frequency effects in eutectic solder alloy. Int J Fatigue 22:217–228
14. Engelmaier W (1983) Fatigue life of leadless chip carrier solder joints during power cycling. IEEE Trans Compon Hybrids Manuf Technol 6:52–57
15. Lin YJ (2000) Board level reliability of chip scale package under cyclic thermomechanical loading, Master Thesis, Department of Mechanical Engineering, National Cheng Kung University
16. Darveaux R (2002) Effect of simulation methodology on solder joint crack growth correlation and fatigue life prediction. J Electron Packag 124:147–154
17. Miner M (1945) Cumulative damage in fatigue. ASME J Appl Mech 12:A159–A164
18. Hamasha S, Jaradat Y, Qasaimeh A, Obaidat M, Borgesen P (2014) Assessment of solder joint fatigue life under realistic service conditions. J Electron Mater 43:4472–4486
19. Su S, Akkara FJ, Thaper R, Alkhazali A, Hamasha M, Hamasha S (2019) A state-of-the-art review of fatigue life prediction models for solder joint. J Electron Packag 141:21–34
20. Hong L-C (2004) Study of warpage due to P-V-T-C relation of EMC in IC packaging, Doctoral Thesis, Department of Mechanical Engineering, National Cheng Kung University
21. Anonymous (2000) JESD22-A104-B: Temperature Cycling, JEDEC Solid State Technology Association
22. Farag MM (2006) Quantitative methods of materials selection. Materials and Mechanical Design, pp 466

Publisher's note Springer Nature remains neutral with regard to jurisdictional claims in published maps and institutional affiliations.